galaxies

MDPI

Article

Constraining Neutron-Capture Nucleosynthesis from Surface Chemical Composition of Chemically Peculiar Stars: The Puzzling Case of HE 1005-1439

Aruna Goswami [1,2,*], Arthur Choplin [3,4], Partha Pratim Goswami [5], Lionel Siess [3,4] and Stephane Goriely [3,4]

1 Indian Institute of Astrophysics, Bangalore 560034, India
2 Institute of Frontier Science and Application, Bangalore 560037, India
3 Institut d'Astronomie et d'Astrophysique, Université Libre de Bruxelles, CP 226, B-1050 Brussels, Belgium; arthur.choplin@ulb.be (A.C.); lionel.siess@ulb.be (L.S.); stephane.goriely@ulb.be (S.G.)
4 BLU-ULB, Brussels Laboratory of the Universe, B-1050 Brussels, Belgium
5 Department of Physics, Dakshin Kamrup College, Gauhati University, Guwahati 781125, India; partha.goswami.iiap@gmail.com
* Correspondence: aruna@iiap.res.in

Abstract

The chemical composition of stellar atmospheres provides a valuable window into the complex processes of stellar nucleosynthesis. Among chemically peculiar cool stars, many objects are the products of mass transfer in binary systems, including most carbon stars, CH stars, and CEMP-*s* and CEMP-*r*/*s* stars. Accurate and precise determinations of heavy-element abundances in these systems serve as powerful tracers of neutron-capture nucleosynthesis operating in the slow (*s*) and intermediate (*i*) regimes. Such measurements also place important constraints on binary evolution, mass-transfer mechanisms, the onset of early *s*-process enrichment, and the astrophysical sites and production pathways associated with the *i*-process. In this work, we investigate the origin of the extremely metal-poor star HE 1005-1439, which has previously been suggested to exhibit a surface composition enriched by a combination of *s*- and *i*-process nucleosynthesis. Using new multi-zone, detailed AGB models for both the *s*- and *i*-processes, we find that a mixed $i + s$ scenario provides a plausible explanation for the observed abundance pattern of HE 1005-1439, although a pure *i*-process AGB model yields an almost equally satisfactory fit.

Keywords: stars: nucleosynthesis; stars: metal-poor; stars: chemical abundances; stars: chemical peculiarity

Check for updates

Academic Editor: Sun Kwok

Received: 7 January 2026
Revised: 31 March 2026
Accepted: 20 April 2026
Published: 23 April 2026

1. Introduction

The chemical diversity observed in the photospheres of cool, evolved stars provides a unique window into the nucleosynthetic processes that have shaped the chemical enrichment of the Galaxy. The majority of chemically peculiar cool stars (CPCSs) exhibit anomalous enhancements of heavy elements produced through neutron-capture reactions. The discovery of barium stars [1] marked the first recognition of this peculiarity. Subsequent identification of CH stars, CEMP-*s* stars, and CEMP-*r*/*s* stars extended this phenomenon to low-metallicity regimes, demonstrating that neutron-capture enrichment occurs across a wide range of stellar ages and Galactic environments.

High-velocity ($V_r > 100$ km s^{-1}) CH stars ($-2 \leq$ [Fe/H] ≤ -0.2) are predominantly members of the Galactic halo with C/O > 1, while CEMP-*s* stars represent the metal-poor analogues of Ba and CH stars [2,3]. Long-term radial velocity studies of CH stars [4] and CEMP-*s* stars [2,5–7] indicate that these objects are mostly members of binary systems.

Comparisons of observed abundances in CEMP-*s* stars with theoretical AGB model predictions confirm that their peculiar surface compositions result from binary mass transfer from an evolved AGB companion [8–18].

CEMP-*r*/*s* stars, in contrast, exhibit enhancements in both slow (*s*-) and rapid (*r*-) neutron-capture process elements. Possible scenarios to explain these abundance patterns include a combination of *r*- and *s*-process nucleosynthesis, or an intermediate neutron-capture process (*i*-process). Proposed astrophysical sites for the *i*-process include AGB stars, e.g., [19,20], rapidly accreting white dwarfs (RAWDs; e.g., [21]), and low-metallicity massive stars, e.g., [22]. Many studies have successfully used *i*-process yields from simplified one-zone or multi-zone models of AGB stars, RAWDs, or massive stars to reproduce the observed abundance patterns of CEMP-*r*/*s* stars, e.g., [14–17,20,23–27].

CEMP-*r* stars, which are enhanced in *r*-process elements, are relatively rare, and their origin remains uncertain.

The present work focuses on the rare object HE 1005-1439. Goswami and Goswami [18] identified HE 1005-1439 as a chemically peculiar, carbon-enhanced, extremely metal-poor star with [C/Fe] = 2.37 and [Fe/H] = −3.03. Slow neutron-capture elements are significantly enhanced, with [Ba/Fe] = 1.16 ± 0.31 and [Pb/Fe] = 1.98 ± 0.19, while the rapid neutron-capture element europium is also enhanced, with [Eu/Fe] = 0.46 ± 0.22.

Based on the classification criteria for CEMP stars, HE 1005-1439 can be categorized as a CEMP-*s* star. However, parametric model-based analyses by Goswami & Goswami indicate that its surface chemical composition reflects comparable contributions from both the *s*- and *i*-processes. Han et al. [28], using different models, suggest that the neutron-capture element abundances arise primarily from the *s*-process in the AGB companion, with additional contributions from *r*-process nucleosynthesis. Using a combination of *s*- and *r*-process abundances, previous studies were able to reproduce the observed patterns of neutron-capture elements. However, the discrepancies noted between these studies motivate a renewed investigation into the astrophysical origin of HE 1005-1439's peculiar abundance pattern. In Section 2, we provide a brief summary of previous work on this object. Section 3 presents our new results based on a model-driven analysis of the observed abundances using multi-zone, detailed *s*-process and *i*-process AGB models. Finally, conclusions are drawn in Section 4.

2. HE 1005-1439: A Brief Summary of Previous Studies

Although HE 1005-1439 has been included in several studies [29–32], only the barium abundance among the neutron-capture elements was reported. Goswami and Goswami [18] derived atmospheric parameters and abundances for ten light and twelve heavy elements, assuming LTE, and discussed potential NLTE effects on selected elements (Na, Mg, Co, and Mn) using results from the literature on metal-poor stars. The star's position on the H-R diagram (log(T_{eff}) vs. log($L/L_{\odot}$)) indicates that it is on the red giant branch.

Based on the CEMP classification criteria of Goswami et al. [17], HE 1005-1439 is classified as a CEMP-*s* star. However, its heavy-to-light *s*-process abundance ratio [hs/ls] ≈ 0.92, where the hs elements include Ba, La, Ce, and Nd, and the ls elements include Sr and Y, is closer to the characteristic peak value of CEMP-*r*/*s* stars (∼1.06; Goswami et al. [17]). Furthermore, comparisons with *s*-process yields from FRUITY models covering a range of stellar masses, e.g., [33–36] at the same metallicity as the programme star ($Z = 2 \times 10^{-5}$) indicate that the observed heavy-element abundance pattern cannot be reproduced [18]. The AGB *s*-process models systematically overproduce the light *s*-process elements Sr and Y, as well as the third-peak element Pb, while underproducing Pr, Er, and Hf. Moreover, the

https://doi.org/10.3390/galaxies14030037

heavy-element abundance pattern cannot be adequately matched by the *i*-process models of Hampel et al. [23] alone, across neutron densities of $n = 10^{12}$–10^{15} cm^{-3}.

To assess the relative contributions of the *s*-, *i*-, and *r*-processes to the observed heavy-element abundances, these authors carried out a parametric-model study using *s*-process yields from FRUITY models spanning different stellar masses ($M = 1.3$–$2.0\,M_{\odot}$), the Solar System *r*-process residual pattern from Arlandini et al. [37], and *i*-process model yields from Hampel et al. [23] at neutron densities of $n = 10^{12}$–10^{15} cm^{-3}.

Lead (Pb) was excluded from the parametric-model analysis because *i*-process yields for this element are not reported by Hampel et al. [23]. The observed elemental abundances of HE 1005-1439, normalized to its La abundance, were then fitted using the parametric model function:

$$\log \epsilon_j = C_s N_{sj} + C_i N_{ij} + C_r N_{rj},$$

where N_{sj}, N_{ij}, and N_{rj} are the normalized abundances from the *s*-, *i*-, and *r*-processes, respectively, and C_s, C_i, and C_r denote the corresponding component coefficients. The minimum χ^2 was achieved for a combination of an *s*-process model with $M = 2.0\,M_{\odot}$ and an *i*-process model with a neutron density of 10^{14} cm^{-3}, with no contribution from the *r*-process. The best-fit parametric model indicates comparable contributions from the *s*- and *i*-processes, with $C_s = 0.56$ and $C_i = 0.44$.

The carbon isotopic ratio ^{12}C/^{13}C is a key diagnostic for understanding the origin of abundance patterns in CEMP stars. For HE 1005-1439, the estimated ^{12}C/^{13}C ratio is low ($\sim$5), much smaller than typical values in intrinsic AGB stars, indicating an extrinsic origin for both its carbon and heavy elements. Furthermore, variations in the radial velocities measured across multiple epochs suggest the presence of a binary companion. Taking these observations into account, Goswami and Goswami [18] proposed that HE 1005-1439 formed through mass transfer from an extinct AGB companion that experienced both *i*- and *s*-process nucleosynthesis. Proton-ingestion episodes (PIEs) likely triggered the *i*-process, while subsequent AGB evolution produced *s*-process material through a few third dredge-up events.

Using the same elemental abundance estimates reported by Goswami and Goswami [18], Han et al. [28] independently investigated the origin of neutron-capture elements in HE 1005-1439. They analyzed the observed abundance pattern using a parameterized four-component model that includes contributions from the main *r*-, weak *r*-, main *s*-, and weak *s*-processes.

Employing a hybrid model that combines *s*- and *r*-process contributions, Han et al. [28] were able to reproduce the neutron-capture abundance pattern of the star. In particular, they used a $2.0\,M_{\odot}$ AGB model at [Fe/H] $= -2.6$ from Bisterzo et al. [38], with abundances scaled to the Solar System *s*-process Ba abundance for the ST/12 case (where ST denotes the standard case). This model yields predicted abundance ratios of [Sr/Ba] $= -0.84$ and [Ba/Pb] $= -0.64$, which are in closest agreement with the observed values compared to other models considered. The resulting fits are consistent with the observed abundances within the uncertainties, including that of Pb. Based on these results, Han et al. [28] concluded that the heavy-element abundances of HE 1005-1439 are predominantly shaped by the *s*-process, with a minor contribution from the *r*-process.

We note that the choice of model database (e.g., FRUITY, Bisterzo-type grids, or other AGB yield sets) typically introduces systematic abundance differences in order 0.2–0.5 dex. For certain elements—particularly Pb, Rb, and the light-*s* elements—these differences can significantly affect the inferred progenitor mass, metallicity, and dominant neutron source. These discrepancies arise primarily from differences in the underlying physical assumptions of the models, including the treatment of the ^{13}C pocket, convective boundary mixing, mass-loss prescriptions, and nuclear reaction rates. Such variations directly influence the predicted neutron exposure and element-by-element yields, thereby affecting the overall quality of the abundance fits, the location of the χ^2 minimum, and the inferred best-fit parameters.

Several studies, including Cseh et al. [39], have demonstrated how differences among AGB yield grids impact the interpretation of observed abundance patterns and the derived progenitor properties of chemically peculiar stars. In particular, FRUITY models generally predict lower Pb abundances and a weaker *s*-process efficiency at low metallicity compared to Bisterzo-type post-processed models, leading to systematic offsets at the level of ∼0.2–0.5 dex.

These considerations highlight that abundance fitting is not model-independent. In this work, we employ multi-zone, detailed *s*-process and *i*-process AGB models to investigate the observed abundance pattern.

3. A Re-Look at the Origin of Neutron-Capture Elements in HE 1005-1439

3.1. Stellar Models

To investigate whether the AGB mass-transfer scenario can account for the abundances of HE 1005-1439, we compare the current observations with AGB nucleosynthesis predictions computed with the STAREVOL code [40,41]. We considered AGB models that undergo either only the *s*-process or only the *i*-process. In our *i*-process models specifically, we do not include mixing below the convective envelope to form the ^{13}C pocket required for radiative *s*-process nucleosynthesis. In the low-metallicity regime considered here ($-3 < [\mathrm{Fe/H}] < -2$), proton-ingestion events (PIEs) are most likely to occur during the first or second AGB thermal pulse, leading to a substantial enrichment of the AGB envelope in heavy elements, as well as in C, N, O, and other species. The increased metal content makes the envelope more opaque, which in turn triggers strong mass loss that can completely remove the envelope before the next thermal pulse in AGB stars with initial masses below roughly 2 $M_\odot$. In more massive AGB stars (∼2 $M_\odot$ and above), the normal TP-AGB phase can resume after the PIE, allowing the radiative *s*-process to occur if a ^{13}C pocket is present. However, at low metallicity, the *i*-process enrichment is typically so large that any subsequent *s*-process may contribute only marginally to the heavy-element distribution. That said, comprehensive models that consistently treat both processes in detail have yet to be developed, and mixed s- and *i*-process contributions cannot be ruled out.

The *s*-process models correspond to AGB stars with an initial mass of 2 $M_\odot$ and metallicities in the range $-3 \leq [\mathrm{Fe/H}] \leq -2$, consistent with the metallicity of HE 1005-1439. They include overshooting below the convective envelope following the prescription of [42]

$$D_{\mathrm{over}} = D_{\mathrm{min}} \times \left(\frac{D_{\mathrm{cb}}}{D_{\mathrm{min}}}\right)^{(1-z/z^*)^p},$$

where the characteristic length z^* is defined as $z^* = f_{\mathrm{over}}\, H_p\, \ln(D_{\mathrm{cb}})/2$. Here, D_{min} denotes the diffusion coefficient at the boundary $z = z^*$, and p is an additional free parameter that sets the slope of the exponential decline of D_{over} as a function of z. In the present *s*-process models, we adopt $f_{\mathrm{over}} = 0.14$, $D_{\mathrm{over}} = 10^7$ cm^2 s^{-1}, and $p = 5$, which lead to efficient radiative *s*-processing with peak neutron densities of order 10^8 cm^{-3}. More details can be found in [42].

For *i*-process models, we explored initial AGB masses in the range $1 < M_{\mathrm{ini}} < 2\, M_\odot$ and metallicities $-3 \leq [\mathrm{Fe/H}] \leq -2$. As detailed in [43], we considered different overshoot strengths above the AGB thermal pulse (but not below the convective envelope), adopting values in the range $0 < f_{\mathrm{over}} < 0.10$, while keeping $p = 1$ and $D_{\mathrm{over}} = 1$ cm^{2}s^{-1}. The maximal neutron density of these models reaches 10^{13-15} cm^{-3}. These models employ a reaction network of 1160 nuclei linked by 2123 reactions. The network accounts for neutron, proton, and α-captures as well as α-decays, weak interactions (electron captures and β-decays), and electromagnetic processes. It includes all nuclei with half-lives typically longer than 1 s and can therefore model neutron-capture processes with neutron densities up to about 10^{17} cm^{-3}. Further details on the models are provided in [20,43,44].

3.2. The Fitting Procedure

To reproduce the chemical abundances of HE 1005-1439, we follow the fitting procedure described in Choplin et al. [20] (Section 6.2). The optimal *s*-process and *i*-process AGB models are identified by minimizing the χ^2 value that quantifies the mismatch between the observed and predicted abundances. The minimum χ^2 is obtained by mixing a fraction of the AGB ejecta into the envelope of the companion star. The dilution factor f, varied freely between 0 and 1, determines the amount of AGB material incorporated into the envelope. Only elements heavier than zinc, with atomic numbers $30 < Z < 83$, are included in the determination of the minimum χ^2. Elements from sodium ($Z = 11$) to zinc are only weakly affected by nucleosynthesis in low-mass AGB stars, and their abundances in the stellar envelope may instead reflect earlier enrichment of the proto-stellar material, for example by winds or core-collapse supernovae from massive stars. The abundances of C, N, and O are more difficult to interpret, as they may have been modified by nucleosynthesis in the AGB donor, may have a non-solar distribution in the proto-stellar cloud, or may have been altered by internal mixing processes during the evolution of the observed star (e.g., after it ascended the giant branch). For completeness, we also performed fits including all available elements in the χ^2 calculation (Section 3.3).

While very few AGB *i*-process predictions are available in the literature, several sets of *s*-process AGB models exist, e.g., [19,38,45] and may influence the fitting results, as these models rely on different input physics, prescriptions for the ^{13}C pocket, and related assumptions.

3.3. Fitting Results: Pure s-Process, Pure i-Process, and Mixed Scenarios

The best-fitting *i*-process model corresponds to a 1 $M_\odot$ AGB star at $[\mathrm{Fe/H}] = -2.5$ with $f_{\mathrm{over}} = 0.04$ (black pattern in Figure 1), whereas the best *s*-process model is a 2 $M_\odot$ AGB star at the same metallicity (blue pattern). The *i*-process model yields a smaller χ^2 value than the *s*-process model (10.48 vs. 16.49; see Figure 1). The higher χ^2 of the *s*-process model arises mainly from Sr and Y, which are overproduced by about 0.5 dex.

As a test, we recomputed the minimum χ^2 including all observed elements. In this case, the best *s*-process model remains the one shown in Figure 1, yielding $\chi^2 = 47$, whereas the best *i*-process model is instead a 2 $M_\odot$ AGB star at $[\mathrm{Fe/H}] = -3$ with $f_{\mathrm{top}} = 0$, giving $\chi^2 = 57$.

We also explored combinations of different nucleosynthetic contributions, namely $s + r$, $i + r$, and $i + s$ mixtures. The *s*- and *i*-process components correspond to the AGB models described above, while the *r*-process abundances are taken from [46]. In these mixed scenarios, two dilution factors, f_1 and f_2, are adjusted (instead of a single one previously) in order to minimize the χ^2 value. For the $s + r$ case, for example, the mass fraction X_i of isotope i is computed as

$$X_i = \left[X_i^{\mathrm{s-pro}}(1 - f_1) + X_i^{\mathrm{ini}} f_1\right](1 - f_2) + X_i^{\mathrm{r-pro}} f_2, \quad (1)$$

where $X_i^{\mathrm{s-pro}}$, X_i^{ini}, and $X_i^{\mathrm{r-pro}}$ denote the mass fractions of isotope i for the *s*-process component, the initial composition, and the *r*-process contribution, respectively. Analogous expressions apply for the $i + r$ and $i + s$ combinations. We emphasize that this represents a simplified approach that does not account for the possible interplay between, for example, the *s*- and *i*-processes that may occur within the same AGB star. Future nucleosynthesis models will aim to combine these processes self-consistently and thereby improve the physical realism of such fits.

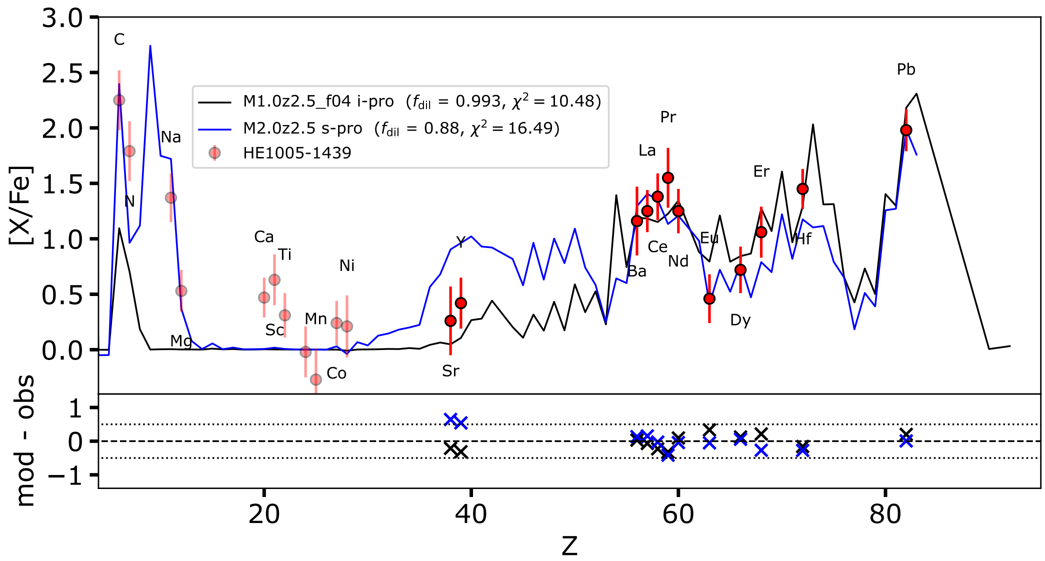

Figure 1. Best-fitting AGB *i*-process (black) and *s*-process (blue) abundance patterns for HE 1005-1439. The black curve represents a 1 $M_\odot$ *i*-process-only AGB model at [Fe/H] = -2.5, while the blue curve corresponds to a 2 $M_\odot$ *s*-process-only AGB model at the same metallicity [Fe/H] = -2.5. The red circles with error bars denote the observed abundances. Shaded circles indicate elements that were not included in the fitting procedure (see text for further details).

Figure 2 shows that all combinations provide a reasonable fit to the heavy-element abundances. We note that the best $i + r$ model is simply the pure *i*-process solution, as adding any *r*-process contribution worsens the agreement with the observations. The overall best fit—particularly for Sr and Y—is obtained with the $i + s$ combination (blue), which yields the lowest χ^2_ν. Interestingly, this model also reproduces the light elements reasonably well, with the exception of nitrogen, which remains underproduced by about 1 dex.

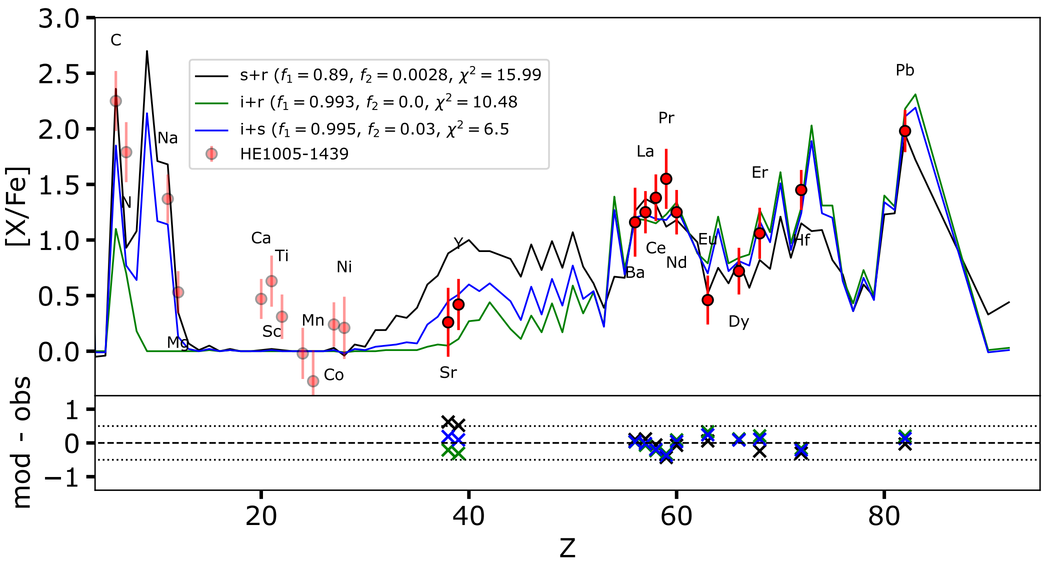

Figure 2. Same as Figure 1, but now showing three different mixed scenarios: $s + r$ (black), $i + r$ (green), and $i + s$ (blue). The red circles with error bars denote the observed abundances. Shaded circles indicate elements that were not included in the fitting procedure (see text for details).

https://doi.org/10.3390/galaxies14030037

4. Concluding Remarks

These results suggest that either a pure *i*-process pattern or a mixed $i + s$ scenario can account for the heavy-element abundances of HE 1005-1439. This is consistent with the parametric model–based results of Goswami and Goswami, which indicate that the surface chemical composition of HE 1005-1439 reflects comparable contributions from both the *s*- and *i*-processes. Accordingly, the mass transfer from a now-extinct AGB companion that experienced both *i*- and *s*-process nucleosynthesis at different evolutionary stages remains a plausible explanation for the peculiar abundance pattern observed in this star. Moreover, the observational constraints provided by this rare object may offer valuable insights into the interplay between PIEs and partial proton mixing in the intershell region and may help explain the overlap in [hs/ls] ratios between CEMP-*s* and CEMP-r/s stars. A more definitive conclusion, however, will require self-consistent AGB models that simultaneously follow both *i*- and *s*-process nucleosynthesis. From an observational perspective, a measurement of the Ta ($Z = 73$) abundance would be particularly valuable, as tantalum is a strong diagnostic of *i*-process nucleosynthesis. Additional constraints could also be obtained from the isotopic ratios of barium or europium [20,47], as well as from the lithium abundance of HE 1005-1439. If not destroyed, lithium may indeed be present in CEMP-r/s stars, as it is expected to be produced in significant quantities during the proton-ingestion events experienced by the AGB donor [26,48]. We further note that the present study is based on LTE abundance estimates, whereas NLTE effects are expected to influence these determinations. For barium, NLTE effects typically lead to positive abundance corrections in giant stars, while europium is generally less sensitive to NLTE effects in cool, low-gravity atmospheres. Consequently, incorporating NLTE effects in abundance analyses of giant stars is likely to improve the reliability of the inferred abundance patterns. Nevertheless, the literature currently provides only a limited number of NLTE abundance measurements for CEMP stars, restricted to a small set of heavy elements derived from high-resolution, high signal-to-noise spectra.

Author Contributions: Conceptualization, A.G.; methodology, A.G. and A.C.; validation, A.G. and A.C.; formal analysis, A.G. and A.C.; investigation, A.G., A.C., P.P.G., L.S. and S.G.; resources, A.G., A.C., P.P.G., L.S. and S.G.; writing, original draft preparation, A.G. and A.C.; writing, review and editing, all authors. All authors have read and agreed to the published version of the manuscript.

Funding: This research received no external funding.

Data Availability Statement: Most data and codes are publicly available.

Acknowledgments: This work made use of the SIMBAD astronomical database, operated at CDS, Strasbourg, France, the NASA ADS, USA and data from the European Space Agency (ESA) mission Gaia https://www.cosmos.esa.int/gaia (accessed on 19 December 2025), processed by the Gaia Data Processing and Analysis Consortium (DPAC, https://www.cosmos.esa.int/web/gaia/dpac/consortium, accessed on 19 December 2025). AG would like to thank the organizers for their kind support and hospitality during the sirEN conference. This work was supported by the Fonds de la Recherche Scientifique-FNRS under Grant No. IISN 4.4502.19. L.S. and S.G. are senior F.R.S-FNRS research associates. A.C. is post-doctorate F.R.S-FNRS fellow.

Conflicts of Interest: The authors declare no conflicts of interest.

Abbreviations

The following abbreviations are used in this manuscript:

CPCS	Chemically peculiar cool star
CEMP	Carbon-enhanced metal-poor star
LTE	Local thermodynamic equilibrium

NLTE	Non-local thermodynamic equilibrium
RAWDs	Rapidly accreting white dwarfs
TP-AGB	Thermally Pulsing Asymptotic Giant Branch

References

1. Bidelman, W.P.; Keenan, P.C. The Ba II Stars. *Astrophys. J.* **1951**, *114*, 473. [CrossRef] [PubMed]
2. Lucatello, S.; Tsangarides, S.; Beers, T.C.; Carretta, E.; Gratton, R.G.; Ryan, S.G. The Binary Frequency Among Carbon-enhanced, *s*-process-rich, Metal-poor Stars. *Astrophys. J.* **2005**, *625*, 825–832. [CrossRef]
3. Abate, C.; Stancliffe, R.J.; Liu, Z.W. How plausible are the proposed formation scenarios of CEMP-r/s stars? *Astron. Astrophys.* **2016**, *587*, A50. [CrossRef]
4. McClure, R.D.; Woodsworth, A.W. The Binary Nature of the Barium and CH Stars. III. Orbital Parameters. *Astrophys. J.* **1990**, *352*, 709. [CrossRef]
5. Starkenburg, E.; Shetrone, M.D.; McConnachie, A.W.; Venn, K.A. Binarity in carbon-enhanced metal-poor stars. *Mon. Not. R. Astron. Soc.* **2014**, *441*, 1217–1229. [CrossRef]
6. Jorissen, A.; Van Eck, S.; Van Winckel, H.; Merle, T.; Boffin, H.M.J.; Andersen, J.; Nordström, B.; Udry, S.; Masseron, T.; Lenaerts, L.; et al. Binary properties of CH and carbon-enhanced metal-poor stars. *Astron. Astrophys.* **2016**, *586*, A158. [CrossRef]
7. Hansen, T.T.; Andersen, J.; Nordström, B.; Beers, T.C.; Placco, V.M.; Yoon, J.; Buchhave, L.A. The role of binaries in the enrichment of the early Galactic halo. II. Carbon-enhanced metal-poor stars: CEMP-no stars. *Astron. Astrophys.* **2016**, *586*, A160. [CrossRef]
8. Busso, M.; Gallino, R.; Wasserburg, G.J. Nucleosynthesis in Asymptotic Giant Branch Stars: Relevance for Galactic Enrichment and Solar System Formation. *Annu. Rev. Astron. Astrophys.* **1999**, *37*, 239–309. [CrossRef]
9. Busso, M.; Gallino, R.; Lambert, D.L.; Travaglio, C.; Smith, V.V. Nucleosynthesis and Mixing on the Asymptotic Giant Branch. III. Predicted and Observed *s*-process Abundances. *Astrophys. J.* **2001**, *557*, 802–821. [CrossRef]
10. Cristallo, S.; Karinkuzhi, D.; Goswami, A.; Piersanti, L.; Gobrecht, D. Constraints of the Physics of Low-mass AGB Stars from CH and CEMP Stars. *Astrophys. J.* **2016**, *833*, 181. [CrossRef]
11. Bisterzo, S.; Gallino, R.; Straniero, O.; Cristallo, S.; Käppeler, F. The *s*-process in low-metallicity stars - II. Interpretation of high-resolution spectroscopic observations with asymptotic giant branch models. *Mon. Not. R. Astron. Soc.* **2011**, *418*, 284–319. [CrossRef]
12. Placco, V.M.; Frebel, A.; Beers, T.C.; Karakas, A.I.; Kennedy, C.R.; Rossi, S.; Christlieb, N.; Stancliffe, R.J. Metal-poor Stars Observed with the Magellan Telescope. I. Constraints on Progenitor Mass and Metallicity of AGB Stars Undergoing *s*-process Nucleosynthesis. *Astrophys. J.* **2013**, *770*, 104. [CrossRef]
13. Hollek, J.K.; Frebel, A.; Placco, V.M.; Karakas, A.I.; Shetrone, M.; Sneden, C.; Christlieb, N. The Chemical Abundances of Stars in the Halo (CASH) Project. III. A New Classification Scheme for Carbon-enhanced Metal-poor Stars with *s*-process Element Enhancement. *Astrophys. J.* **2015**, *814*, 121. [CrossRef]
14. Shejeelammal, J.; Goswami, A.; Goswami, P.P.; Rathour, R.S.; Masseron, T. Characterizing the companion AGBs using surface chemical composition of barium stars. *Mon. Not. R. Astron. Soc.* **2020**, *492*, 3708–3727. [CrossRef]
15. Shejeelammal, J.; Goswami, A. Probing the Nucleosynthetic Contribution of Low-metallicity, Low-mass Star Companions of CEMP Stars. *Astrophys. J.* **2021**, *921*, 77. [CrossRef]
16. Shejeelammal, J.; Goswami, A. Spectroscopic Study of Four Metal-poor Carbon Stars from the Hamburg/ESO Survey: On Confirming the Low-mass Nature of Their Companions. *Astrophys. J.* **2022**, *934*, 110. [CrossRef]
17. Goswami, P.P.; Rathour, R.S.; Goswami, A. Spectroscopic study of CEMP-(s & r/s) stars. Revisiting classification criteria and formation scenarios, highlighting *i*-process nucleosynthesis. *Astron. Astrophys.* **2021**, *649*, A49. [CrossRef]
18. Goswami, P.P.; Goswami, A. The peculiar abundances of HE 1005-1439. A carbon-enhanced extremely metal-poor star contaminated with products of both s- and *i*-process nucleosynthesis. *Astron. Astrophys.* **2022**, *657*, A50. [CrossRef]
19. Cristallo, S.; Piersanti, L.; Straniero, O.; Gallino, R.; Domínguez, I.; Käppeler, F. Asymptotic-Giant-Branch Models at Very Low Metallicity. *Publ. Astron. Soc. Aust.* **2009**, *26*, 139–144. [CrossRef]
20. Choplin, A.; Siess, L.; Goriely, S. The intermediate neutron capture process. I. Development of the *i*-process in low-metallicity low-mass AGB stars. *Astron. Astrophys.* **2021**, *648*, A119. [CrossRef]
21. Denissenkov, P.A.; Herwig, F.; Battino, U.; Ritter, C.; Pignatari, M.; Jones, S.; Paxton, B. *i*-process Nucleosynthesis and Mass Retention Efficiency in He-shell Flash Evolution of Rapidly Accreting White Dwarfs. *Astrophys. J. Lett.* **2017**, *834*, L10. [CrossRef]
22. Clarkson, O.; Herwig, F.; Pignatari, M. Pop III *i*-process nucleosynthesis and the elemental abundances of SMSS J0313-6708 and the most iron-poor stars. *Mon. Not. R. Astron. Soc.* **2018**, *474*, L37–L41. [CrossRef]

https://doi.org/10.3390/galaxies14030037

23. Hampel, M.; Stancliffe, R.J.; Lugaro, M.; Meyer, B.S. The Intermediate Neutron-capture Process and Carbon-enhanced Metal-poor Stars. *Astrophys. J.* **2016**, *831*, 171. [CrossRef]
24. Hampel, M.; Karakas, A.I.; Stancliffe, R.J.; Meyer, B.S.; Lugaro, M. Learning about the Intermediate Neutron-capture Process from Lead Abundances. *Astrophys. J.* **2019**, *887*, 11. [CrossRef]
25. Karinkuzhi, D.; Van Eck, S.; Goriely, S.; Siess, L.; Jorissen, A.; Merle, T.; Escorza, A.; Masseron, T. Low-mass low-metallicity AGB stars as an efficient *i*-process site explaining CEMP-rs stars. *Astron. Astrophys.* **2021**, *645*, A61. [CrossRef]
26. Choplin, A.; Siess, L.; Goriely, S.; Martinet, S. Production of Lithium and Heavy Elements in AGB Stars Experiencing PIEs. *Galaxies* **2024**, *12*, 66. [CrossRef]
27. Riyas, A.M.; Karinkuzhi, D.; Van Eck, S.; Choplin, A.; Goriely, S.; Siess, L.; Keerthy, M.V.; Jorissen, A.; Merle, T. Abundance of heavy *r*-process elements in CEMP-rs stars: The role of the *i*-process. *arXiv* **2025**, arXiv:2510.13339. [CrossRef]
28. Han, W.Q.; Yang, G.C.; Niu, P.; Zhang, B. Study of the Astrophysical Origins of Neutron-capture Elements in CEMP Star HE 1005-1439. *Chin. Astron. Astrophys.* **2024**, *48*, 73–83. [CrossRef]
29. Aoki, W.; Beers, T.C.; Christlieb, N.; Norris, J.E.; Ryan, S.G.; Tsangarides, S. Carbon-enhanced Metal-poor Stars. I. Chemical Compositions of 26 Stars. *Astrophys. J.* **2007**, *655*, 492–521. [CrossRef]
30. Schuler, S.C.; Margheim, S.J.; Sivarani, T.; Asplund, M.; Smith, V.V.; Cunha, K.; Beers, T.C. Carbon Abundances of Three Carbon-Enhanced Metal-Poor Stars from High-Resolution Gemini-S/bHROS Spectra of the λ8727 [C I] Line. *Astron. J.* **2008**, *136*, 2244–2258. [CrossRef]
31. Yong, D.; Norris, J.E.; Bessell, M.S.; Christlieb, N.; Asplund, M.; Beers, T.C.; Barklem, P.S.; Frebel, A.; Ryan, S.G. The Most Metal-poor Stars. II. Chemical Abundances of 190 Metal-poor Stars Including 10 New Stars with [Fe/H] ≤ -3.5. *Astrophys. J.* **2013**, *762*, 26. [CrossRef]
32. Caffau, E.; Bonifacio, P.; Starkenburg, E.; Martin, N.; Youakim, K.; Henden, A.A.; González Hernández, J.I.; Aguado, D.S.; Allende Prieto, C.; Venn, K.; et al. The Pristine survey II: A sample of bright stars observed with FEROS. *Astron. Nachrichten* **2017**, *338*, 686–695. [CrossRef]
33. Straniero, O.; Gallino, R.; Cristallo, S. s process in low-mass asymptotic giant branch stars. *Nucl. Phys. A* **2006**, *777*, 311–339. [CrossRef]
34. Cristallo, S.; Straniero, O.; Gallino, R.; Piersanti, L.; Domínguez, I.; Lederer, M.T. Evolution, Nucleosynthesis, and Yields of Low-Mass Asymptotic Giant Branch Stars at Different Metallicities. *Astrophys. J.* **2009**, *696*, 797–820. [CrossRef]
35. Cristallo, S.; Piersanti, L.; Straniero, O.; Gallino, R.; Domínguez, I.; Abia, C.; Di Rico, G.; Quintini, M.; Bisterzo, S. Evolution, Nucleosynthesis, and Yields of Low-mass Asymptotic Giant Branch Stars at Different Metallicities. II. The FRUITY Database. *Astrophys. J. Suppl. Ser.* **2011**, *197*, 17. [CrossRef]
36. Cristallo, S.; Straniero, O.; Piersanti, L.; Gobrecht, D. Evolution, Nucleosynthesis, and Yields of AGB Stars at Different Metallicities. III. Intermediate-mass Models, Revised Low-mass Models, and the ph-FRUITY Interface. *Astrophys. J. Suppl. Ser.* **2015**, *219*, 40. [CrossRef]
37. Arlandini, C.; Käppeler, F.; Wisshak, K.; Gallino, R.; Lugaro, M.; Busso, M.; Straniero, O. Neutron Capture in Low-Mass Asymptotic Giant Branch Stars: Cross Sections and Abundance Signatures. *Astrophys. J.* **1999**, *525*, 886–900. [CrossRef]
38. Bisterzo, S.; Gallino, R.; Straniero, O.; Cristallo, S.; Käppeler, F. *s*-process in low-metallicity stars—I. Theoretical predictions. *Mon. Not. R. Astron. Soc.* **2010**, *404*, 1529–1544. [CrossRef]
39. Cseh, B.; Világos, B.; Roriz, M.P.; Pereira, C.B.; D'Orazi, V.; Karakas, A.I.; Soós, B.; Drake, N.A.; Junqueira, S.; Lugaro, M. Barium stars as tracers of *s*-process nucleosynthesis in AGB stars. I. 28 stars with independently derived AGB mass. *Astron. Astrophys.* **2022**, *660*, A128. [CrossRef]
40. Siess, L.; Dufour, E.; Forestini, M. An internet server for pre-main sequence tracks of low- and intermediate-mass stars. *Astron. Astrophys.* **2000**, *358*, 593–599. [CrossRef]
41. Siess, L. Evolution of massive AGB stars. I. Carbon burning phase. *Astron. Astrophys.* **2006**, *448*, 717–729. [CrossRef]
42. Goriely, S.; Siess, L. Sensitivity of the *s*-process nucleosynthesis in AGB stars to the overshoot model. *Astron. Astrophys.* **2018**, *609*, A29. [CrossRef]
43. Choplin, A.; Siess, L.; Goriely, S.; Martinet, S. The intermediate neutron capture process. V. The *i*-process in AGB stars with overshoot. *Astron. Astrophys.* **2024**, *684*, A206. [CrossRef]
44. Choplin, A.; Siess, L.; Goriely, S. The intermediate neutron capture process. III. The *i*-process in AGB stars of different masses and metallicities without overshoot. *Astron. Astrophys.* **2022**, *667*, A155. [CrossRef]
45. Ritter, C.; Herwig, F.; Jones, S.; Pignatari, M.; Fryer, C.; Hirschi, R. NuGrid stellar data set—II. Stellar yields from H to Bi for stellar models with M_{ZAMS} = 1–25 $M_{\odot}$ and Z = 0.0001–0.02. *Mon. Not. R. Astron. Soc.* **2018**, *480*, 538–571. [CrossRef]
46. Arnould, M.; Goriely, S.; Takahashi, K. The *r*-process of stellar nucleosynthesis: Astrophysics and nuclear physics achievements and mysteries. *Phys. Rep.* **2007**, *450*, 97–213. [CrossRef]

47. Choplin, A.; Goriely, S.; Siess, L.; Martinet, S. Synthesis of actinides and short-lived radionuclides during *i*-process nucleosynthesis in AGB stars. *Eur. Phys. J. A* **2025**, *61*, 68. [CrossRef]
48. Iwamoto, N.; Kajino, T.; Mathews, G.J.; Fujimoto, M.Y.; Aoki, W. Flash-Driven Convective Mixing in Low-Mass, Metal-deficient Asymptotic Giant Branch Stars: A New Paradigm for Lithium Enrichment and a Possible *s*-process. *Astrophys. J.* **2004**, *602*, 377–388. [CrossRef]

https://doi.org/10.3390/galaxies14030037